Lysosome Passivation Triggered by Ag Nanoparticles Enhances Subcellular-Targeted Drug Therapy

Xueqian Wang
Shandong First Medical University
Shulin Zhao
Shandong First Medical University
Guiqian Fang
Shandong First Medical University
Ran Wang
Shandong First Medical University
Xinxing Lyu
Shandong First Medical University
Xintian Shao
Shandong First Medical University
Peixue Ling
Shandong Academy of Pharmaceutical Science, Key Laboratory of Biopharmaceuticals
caicai meng
Shandong First Medical University
Yanling Mu
Shandong First Medical University
Qixin Chen
Shandong First Medical University
Jia Chen (chenjia@sdfmu.edu.cn)
Shandong First Medical University

Research Article

Keywords: lysosome, super-resolution imaging, silver nanoparticles, cancer therapy

Posted Date: December 13th, 2023

DOI: https://doi.org/10.21203/rs.3.rs-3704972/v1

Additional Declarations: No competing interests reported.

Abstract

Background: Frequently, subcellular-targeted drugs tend to accumulate in lysosomes after cellular absorption, a process termed the lysosomal trap. This accumulation often interferes with the drug's ability to bind to its target, resulting in decreased efficiency. Existing methods for addressing lysosome-induced drug resistance mainly involve improving the structures of small molecules or enveloping drugs in nanomaterials. Nonetheless, these approaches can lead to changes in the drug structure or potentially trigger unexpected reactions within organisms.

Results: To address these issues, we introduced a strategy that involves inactivating the lysosome with the use of Ag nanoparticles. In this method, the Ag nanoparticles gradually accumulate inside lysosomes, leading to permeation of the lysosomal membrane and subsequent lysosomal inactivation. Importantly, coincubating nanoparticles with various subcellular-targeted drugs was found to significantly increase the efficiency of these treatments.

Conclusion: Our strategy illustrates the potential of using lysosomal inactivation to enhance drug efficacy, providing a promising therapeutic strategy for cancer.

Introduction

Lysosomes are membrane-bound organelles that contain acidic vesicular compartments that function as recycling centers within cells[1]. Lysosomes receive cargoes from the plasma membrane through endocytosis[2] and from the cytoplasm via autophagy[3], and all of these materials are ultimately destined for degradation and/or recycling[4, 5]. In cancer cells, dysregulation of these degradation pathways leads to alterations in the structure and function of lysosomal membranes. Consequently, cancer cells become more vulnerable to lysosomal membrane permeabilization triggered by various endogenous factors, such as oxidative stress, and exogenous factors, such as cationic amphiphilic drugs.

Oncology treatments encounter inevitable challenges - resistance to conventional chemotherapeutic agents[6] and newer targeted drugs[7]. Such drug resistance remains a leading cause of treatment failure and cancer mortality[8]. Numerous studies have highlighted the critical role of lysosomes in mediating drug resistance in tumors[9-11]. The key issue is that hydrophobic and weakly basic chemotherapeutic agents are sequestered through passive ion trapping, leading to their reduced effectiveness at the target sites[12]. Therefore, enhancing drug release in lysosomes is a promising strategy to improve the efficacy of antitumor drugs[13-16]. Currently, there are two main strategies to address the issue of drug release caused by the lysosomal uptake of drugs[17]. The first strategy involves modifying and optimizing the chemical structure of the drug, such as adding a targeting group[17] or transforming the drug into a prodrug[8]. The second strategy involves leveraging biomedical engineering technology to facilitate drug delivery, such as using nanomaterials or biological materials to encapsulate or load drugs[18, 19].

However, these strategies may have unfavorable effects on the drug, such as the introduction of additional groups, which leads to compromised drug efficacy or an undesired rise in toxicity[20].

To fill up this gap, we proposed a strategy of nanoparticle accumulation to passivate lysosomes to enhance drug delivery effectiveness. Initially, the fluorescent nanoparticles are taken up into the lysosomes of tumor cells through endocytosis. Subsequently, the accumulation of the nanoparticles in the lysosomes triggers lysosomal passivation and leads to gradual membrane permeabilization. Finally, coincubating nanoparticles with various antitumor drugs was found to significantly increase the efficiency of these therapeutic treatments. Our findings suggest that a nanoparticle-triggered lysosomal passivation strategy can practically improve the therapeutic effects of antitumor drugs by overcoming lysosomal sequestration, providing a promising strategy for cancer therapy.

Results and Discussion

Design and characterization of the Cy3.5@Ag NPs

As silver nanoparticles possess the merits of being benign and biocompatible, easily accessible and facilely decorated and previous literature reports have shown that silver nanoparticle treatment may cause lysosome injury[21], we designed Ag-based fluorescent nanoparticles to promote the efficient release of antitumor drugs from the lysosomes. Moreover, the common fluorescent dye Cy3.5 was also incorporated to modify the Ag nanoparticles (generating **Cy3.5@Ag NPs**) for imaging inside the cells. These nanoparticles were synthesized by forming a covalent bond between Cy3.5 and the polyethylene glycol (PEG)-encased silver nanocore (Ag NP) via a universally employed amide linkage that connects the amino group of Cy3.5 with the carboxyl group of the PEG chain (Figure 1A). These nanoparticles preferentially accumulate in lysosomes, instigating lysosomal passivation and lysosomal membrane permeabilization (LMP), which catalyzes the escape of these particles from the lysosomes (Figure 1B).

The cytotoxicity of both the Cy3.5 compound and the **Cy3.5@Ag NPs** was examined by treating HeLa cells with varying concentrations of these samples for a duration of 24 hours. Cytotoxicity was subsequently assessed using CCK-8 kits by measuring the samples' respective optical densities (ODs). The findings revealed that none of the samples inhibited the proliferation of HeLa cells within a specified concentration range (Figures S1 and S2). Consequently, this suggests that both the Cy3.5 compound and the Cy3.5@Ag NPs do not demonstrate any discernible inhibitory effects on cell proliferation, thereby ensuring their safety, and Cy3.5 could serve solely as a fluorescence marker.

Comprising three components—a 15 nm silver core, a biocompatible PEG spacer (5 kD) and the fluorescent dye Cy3.5 (Figure 1A)—the **Cy3.5@Ag NPs** exhibited homogeneous spherical structures. Their size predominantly ranged from 25-45 nm, as observed in the transmission electron microscopy (TEM) images (Figure S3A), while their hydrodynamic radii were approximately near 80-90 nm, as indicated by dynamic light scattering (DLS) (Figure S3B). The photophysical properties of these nanoparticles were scrutinized via UV−vis absorbance spectroscopy and fluorescence spectroscopy, with the Cy3.5@Ag NPs

showing a single peak at 406 nm in the absorbance spectrum (Figure S4A) and emitting intense red fluorescence at approximately 610 nm (Figure S4B).

Localization of the Cy3.5@Ag NPs in the lysosomes

To determine the ability of the nanoparticles to be used for live cell imaging, HeLa cells were incubated with **Cy3.5@Ag NPs** (0.5 μg/ml) for 1 h. We performed SIM imaging in single-channel mode with excitation at 488 nm. After 1 hour of incubation with **Cy3.5@Ag NPs**, we observed conspicuous red fluorescence signals, which presented as evenly dispersed globular particles within the cytoplasm (Figure 2A and 2B). The magnified images further showed distinctive red fluorescence appearing as individually scattered circular spots, consistent with previous literature [22]. Notably, when compared to the nanoparticles, HeLa cells treated with Cy3.5 (0.1 μM) for 1 h demonstrated consistent localization of Cy3.5 in mitochondria (Figure S5). Our results thus confirmed time-dependent variations in the cellular distribution of the **Cy3.5@Ag NPs**.

Given the observed fluorescence distribution of the **Cy3.5@Ag NPs**, we deduced that these NPs likely localized within lysosomes. To substantiate our hypothesis, we administered **Cy3.5@Ag NPs** (0.5 μg/mL) to HeLa cells, and after 1 hour, the cells were treated with the commercially available probe Lyso-Tracker Deep Red (LTDR, 100 nM). As anticipated, the red fluorescence of the **Cy3.5@Ag NPs** showed considerable overlap with the magenta fluorescence of LTDR after 1 hour of incubation, resulting in a Pearson's colocalization coefficient (PCC) of 0.68 (Figure 2C, 2D and 2E).

The confocal microscopy data lent further support to these findings (Figure S6). We also validated the subcellular distribution of the **Cy3.5@Ag NPs** within HT-1080 cells (Figure S7), which demonstrated pronounced colocalization with LTDR. These findings strongly support the hypothesis that **Cy3.5@Ag NPs** localize to lysosomes. Therefore, our study concludes that **Cy3.5@Ag NPs** penetrated living cells and were assimilated by lysosomes.

Cy3.5@Ag NPs induced lysosomal membrane permeabilization and lysosomal passivation

We also assessed how the **Cy3.5@Ag NPs** affect the behavior of lysosomes in live cells, focusing on their selective uptake and subsequent effects on lysosomal membrane integrity. Following treatment with these nanoparticles (0.5 μg/mL, 6 h), we observed sensitization of the HeLa cell lysosomal membranes to damage by photooxidation[23]. This was indicated by an increase in green fluorescence and a decrease in red fluorescence. Time-lapse confocal images of both untreated and treated cells revealed substantial changes in the fluorescence of the lysosomes (red signal) and cytoplasm (green signal) following exposure to the NPs (Figure 3A, 3B and 3C), suggesting that the stability of the lysosomal membrane was impacted. Our findings suggest that **Cy3.5@Ag NPs** induce lysosomal membrane instability and instigate lysosomal evasion (Figure 3D).

When lysosomes absorb nanoparticles, it can lead to a condition known as lysosomal stress, potentially causing the lysosomes to swell[24, 25]. Our analysis of the effect of **Cy3.5@Ag NPs** on lysosomal

morphology[26] involved treating HeLa cells with 0.5 μg/mL NPs for 1 hour and LTDR for 30 minutes. Upon examination, we found no signs of lysosomal swelling caused by the NPs. The size distribution of the particles was consistent with standard lysosomal characteristics[22], supporting this conclusion (Figure S8). The morphology was further confirmed by TEM analysis (Figure S9).

To assess the impact of the **Cy3.5@Ag NPs** on lysosomal movement[1] within the cytoplasm, we tracked lysosomal motion using SIM time-lapse photography. Untreated HeLa cells exhibited random movements near the nucleus and more directed movements around the cell, consistent with previous findings[24]. In contrast, the presence of **Cy3.5@Ag NPs** caused significant changes in the movement patterns of the lysosomes, resulting in stable in situ trajectory structures (Figure 4A, 4B and 4C). There was also a noticeable reduction in both the track length and displacement of the lysosomal movements in the cells treated with the NPs (Figure 4D), pointing to a significant decrease in lysosomal motility due to the presence of **Cy3.5@Ag NPs** (Figure 4E).

Investigation of the specificity and selectivity of **Cy3.5@Ag NPs** for the lysosomes in HeLa cells was conducted after demonstrating their lysosomal escape behavior and their effect on inhibiting lysosome mobility. To evaluate the nanoparticles' lysosomal uptake specificity postinternalization, HeLa cells were treated with bafilomycin A1 (BafA1, 100 nM) and chloroquine (CQ, 50.0 μM) for 3 hours to minimize lysosomal uptake[27-29]. Next, the cells were treated with **Cy3.5@Ag NPs** for an hour, after which observations were made via confocal laser scanning microscopy (CLSM). The CLSM images revealed that BafA1 or CQ treatment led to **Cy3.5@Ag NPs** displaying diffuse fluorescence signals in the cytoplasm, replacing the speckled patterns seen in nontreated cells (Figure S10), proving that these nanoparticles are specifically absorbed by lysosomes.

Moreover, the selectivity of these nanoparticles for lysosomes and their safety concerning other organelles were examined by costaining HeLa cells with **Cy3.5@Ag NPs** (λex= 488 nm) and other commercially available probes, such as a nucleus probe (Hoechst, λex=405 nm), a lipid droplet probe (Lipi-Blue, λex=405 nm), and an autophagolysosome probe (DALG, λex= 488 nm). The findings confirmed that the **Cy3.5@Ag NP**s did not invade other organelles (Figures S11-S13). Therefore, collectively, our findings affirm that these **Cy3.5@Ag NPs** selectively target lysosomes without impacting other organelles.

Enhancement of subcellular-targeted drug efficacy facilitated by Cy3.5@Ag NPs

Many existing antitumor drugs are unable to escape from lysosomes after being swallowed[6, 7], resulting in a decrease in efficacy and the development of drug resistance. To assess whether **Cy3.5@Ag NPs** can trigger lysosomal escape, thereby boosting drug release from the lysosomes and amplifying drug effectiveness, we paired them with various traditional antitumor drugs. We then used SIM imaging and cellular toxicity tests to confirm the potential of the **Cy3.5@Ag NPs** to enhance the potency of these antitumor drugs.

Previous research has shown that carbonyl cyanide 3-chlorophenylhydrazone (CCCP), a mitochondria-targeted inhibitor, can inhibit STING-mediated IFN-β production by disrupting the mitochondrial

membrane potential[30]. As illustrated in Figure 5A, HeLa cells were treated with CCCP (5.0 μM), and the mitochondria were labeled with MTG. The results showed that cellular mitochondria were swollen and even fragmented, and more mitochondrial swelling as well as more severe mitochondrial fragmentation was observed after CCCP coincubation with the **Cy3.5@Ag NPs** (0.5 μg/mL). This was evident in MTG-labeled mitochondria determined through aspect ratio analysis plots of the mitochondria in each group (Figure 5C and Figure S14). We speculate that this phenomenon was due to the increased permeability of the lysosomal membrane induced by **Cy3.5@Ag NPs** that facilitated the effective binding of CCCP to the mitochondria, resulting in an enhanced ability to induce mitochondrial autophagy. Moreover, the cellular value-added toxicity assay results also demonstrated that coincubation of **Cy3.5@Ag NPs** with CCCP resulted in lower cell survival than CCCP treatment alone (Figure 5E). Our findings provide compelling evidence that the presence of **Cy3.5@Ag NPs** amplifies the capacity of CCCP to induce mitochondrial autophagy.

Brequinar (BQR), a typical inhibitor of mitochondrial dihydroorotic acid dehydrogenase, can trigger lipid peroxidation-linked iron death by obstructing the fourth step in the pyrimidine de novo synthesis pathway[31, 32]. As illustrated in Figure 5B and 5D, HeLa cells were treated with BQR (40 μM), and mitochondria were labeled with MTG. The results showed that the cellular mitochondria were fibrillated and fragmented, and BQR coincubation with **Cy3.5@Ag NPs** (0.5 μg/mL) resulted in more mitochondrial fibrillation as well as more severe mitochondrial fragmentation. Moreover, the cellular value-added toxicity assay data also demonstrated that coincubation of **Cy3.5@Ag NPs** with BQR resulted in lower cell survival than BQR treatment alone (Figure 5E). All these results suggest that **Cy3.5@Ag NPs** can effectively promote the efficacy of mitochondria-targeted antitumor drugs (Figure 5F and 5G).

Furthermore, in addition to mitochondria-targeted drugs, **Cy3.5@Ag NPs** also have the ability to facilitate the release of nucleus-targeted drugs from the lysosomes. Herein, two nucleus-targeted drugs, adriamycin (ADR) and gemcitabine (GEM), which target DNA and RNA, respectively, were chosen to validate this hypothesis[33, 34]. HeLa cells were treated with ADR (1.0 μM) and **Cy3.5@Ag NPs** (0.5 μg/mL) for 24 h, and cytotoxicity was examined with CCK-8 kits. GEM (10 μM) was analyzed in the same way. The results demonstrated that the utilization of **Cy3.5@Ag NPs** can strengthen the cytotoxicity of ADR and GEM in comparison to ADR and GEM alone (Figure S15), suggesting that the **Cy3.5@Ag NPs** promote drug escape from the lysosome by altering the permeability of the lysosomal membrane. In conclusion, **Cy3.5@Ag NPs** can improve the efficacy of subcellular-targeted drugs while retaining biosafety.

Conclusion

In summary, we have successfully developed a new strategy to enhance drug delivery effectiveness. Silver-based **Cy3.5@Ag NPs,** which act as passivating agents in the chemotherapy process, primarily accumulate in lysosomes, instigate lysosomal membrane permeabilization and lead to lysosomal passivation. The efficacies of various antitumor drugs (carbonyl cyanide 3-chlorophenylhydrazone (CCCP), brequinar, adriamycin and gemcitabine) were significantly improved after coincubation with **Cy3.5@Ag NPs** without any adverse effects. Our findings suggested that the **Cy3.5@Ag NP-**induced

lysosomal passivation strategy can improve the therapeutic effects of antitumor drugs by overcoming lysosomal sequestration, providing a promising strategy for cancer therapy.

Experimental section

General Materials

Carbonyl cyanide 3-chlorophenylhydrazone (#HY-100941, CCCP), brequinar (#HY-108325, BQR), dexrazoxane (#HY-B0581, ADR), gemcitabine (#HY-17026, GEM), bafilomycin A1 (#HY-100558, BAF), and chloroquine (#HY-17589A CQ) were all purchased from MedChemExpress (MCE, China). Mito-Tracker Green (#M7514, MTG), Lyso-Tracker Deep Red (#L12492, LTDR), Lyso-Tracker Blue (#L7525, LTB), and Hoechst 33342 (#62249, Hoechst) were all purchased from Invitrogen (Thermo Fisher Scientific, USA), and Lipi-Blue (#LD01) was purchased from Dojindo (Japan). Acridine orange (#235474, AO) was purchased from Sigma–Aldrich (China). Dulbecco's modified Eagle's medium (#11965092, DMEM), phenol-free medium (#1894117), phosphate-buffered saline (#20012027, PBS), and penicillin–streptomycin (#15140163, 10,000 units/mL) were purchased from Gibco BRL (Thermo Fisher Scientific, China). Fetal bovine serum (#P50304, FBS) was purchased from Cell Box (China). Cell Counting Kit-8 (#BS350B, CCK8) was purchased from Biosharp (China). Dimethyl sulfoxide (#D3871, DMSO) was purchased from Solarbio (China). The nanoparticles were custom synthesized by Xi'an Ruixi Biological Technology Co. (Xi'an, China), and the data characterizing the nanoparticles were also measured by Xi'an Ruixi Biological Technology Co. (Figures S4B and S5). The HeLa cells were a gift from Fengshan Wang's laboratory (Shandong University). HT-1080 (#TCHu170) cells were purchased from the National Collection of Authenticated Cell Cultures (China).

Cell culture

HeLa cells were cultured in Dulbecco's modified Eagle's medium supplemented with 10% fetal bovine serum and 1% penicillin–streptomycin, maintained at 37 °C, and incubated in an atmosphere with 5% CO_2.

Cell staining and imaging

Stock solutions of Cy3.5@Ag NPs (1 mg/mL) in H_2O and the commercial dyes (1×10^{-3} M) in DMSO were prepared. These solutions were then diluted with the HeLa cell culture medium to the desired concentration. The cells were incubated at 37 °C in an environment containing 5% CO_2. A glass-bottom microwell dish was seeded with a total of 1×10^5 HeLa cells. These cells were incubated with 2 mL of DMEM supplemented with 10% FBS at 37 °C in an atmosphere containing 5% CO_2 for 24 h. Next, the cells were stained with Cy3.5@Ag NPs for various lengths of time and with commercial probes for an additional 30 min. After treatment, the cells were washed five times with prewarmed PBS and then three times with prewarmed free DMEM. Finally, the cells were cultured with 1 mL of phenol-free medium and observed using a super-resolution microscope. SIM images were acquired on an Elyra instrument (Carl

Zeiss, ELYRA 7 with Lattice SIM², Germany), employing a 60× oil objective. The images were processed, and the channels were aligned using the automatic settings on the ZEN Black software (Carl Zeiss, Germany). For confocal images, a confocal laser scanning microscope (Carl Zeiss, LSM 980, Germany) was utilized, and the images were analyzed using ImageJ software. The software was equipped with a colocalization analysis plugin to calculate the Pearson's correlation coefficient (PCC), which indicates the degree of overlap between two fluorescent channels based on pixel values.

Cell Viability Assay

HeLa cells were plated onto 96-well plates at a density of 7×10^3 cells per well in DMEM with 10% FBS and incubated at 37 °C for 24 h. Next, the medium was replaced with 100 μL of fresh medium containing various concentrations of **Cy3.5@Ag NPs** (or other drugs). After 24 h of incubation, 10 μL of CCK8 solution was added to each well, and the plate was incubated for an additional 4 h. The absorbance of each well was then measured at 450 nm using an enzyme-linked immunosorbent assay plate reader. To calculate cell viability, the formula mean absorbance value of the treatment group divided by the mean absorbance value of the control group was used.

Determination of lysosomal membrane integrity

Evaluation of the lysosomal membrane integrity was performed by observing live cells and assessing the release of lysosomal acridine orange (AO) into the cytoplasm when exposed to photooxidation. Briefly, cells were grown in cell culture dishes with glass bottoms and treated with **Cy3.5@Ag NPs** (0.5 μg/ml) for 6 h. Subsequently, AO (2 μg/mL) was added directly to the growth medium and allowed to incubate for an additional 20 minutes at 37 °C. Cells were then rinsed three times, the medium was exchanged with PBS containing 3% FBS, and samples were transferred to an LSM 980 laser scanning confocal microscope stage equipped with a 60× oil objective. AO was stimulated using 488 nm light emitted by a laser at an intensity of 2.4%. Lysosomal membrane disruption and AO release into the cytoplasm were observed by capturing time-lapse images every 5 seconds over a total period of 300 seconds using a channel defined by 495-555 nm and 595-645 nm bandpass filters. The green and red fluorescence intensities were measured within specific regions of interest (ROIs), demarcating clusters of cells, using ImageJ software.

Transmission electron microscopy

Cells were exposed to 0.5 μg/ml **Cy3.5@Ag NPs** for different lengths of time, washed with PBS and fixed with 2% glutaraldehyde and 2% paraformaldehyde solution in PBS-sodium cacodylate buffer (50:50). Cells were harvested and postfixed with 2% osmium tetroxide, stained with 2% uranyl acetate and embedded in propylene oxide and Eponate. Samples were examined on HT-7800 electron microscopes.

Data analysis

Statistical analysis was performed using GraphPad Prism 9.4 and Origin 2021. Normality and log-normality tests were used to confirm normal distribution. In the case of a normal distribution, Student's t test was applied statistically compare the results. Data are presented as the mean ± SEM. The SEM was used to compare the experimental results with the controls. In the case of nonnormal distribution, statistical comparison of the results was performed with a Mann—Whitney test, with levels of significance set at n.s. (no significant difference), *$P < 0.05$, **$P < 0.01$, ***$P < 0.001$ and ****$P < 0.0001$. The statistical significance and sample sizes are indicated in the corresponding figure legends of all graphs.

Declarations

Supplementary Information

The online version contains supplementary material available at https://doi.

Acknowledgements

Not applicable.

Authors' contributions

Xueqian Wang, Jia Chen and CaiCai Meng conceived and designed the analysis; Xueqian Wang, Shulin Zhao and Xinxing Lyu collected the data; Guiqian Fang, Ran Wang and Xintian Shao contributed data or analysis tools; Xueqian Wang, Yanling Mu, Peixue Ling and Jia Chen performed the analysis; Xueqian Wang, CaiCai Meng and Yanling Mu wrote the paper; Qixin Chen provided the funding.

Funding

This work was financially supported the Shandong Province Key R&D Program (Major Technological Innovation Project) (2021CXGC010501), Chinese Society of Traditional Chinese Medicine Young Talent Support Project (CACM-2023-QNRC1-02), National Natural Science Foundation of China (Nos. 22107059, 22007060), Natural Science Foundation of Shandong Province (ZR2021QH057, ZR2022QH304, ZR2020QB166), Innovation Team of Shandong Higher School Youth Innovation Technology Program (2021KJ035), Taishan Scholars Program (TSQN202211221), Taishan Scholars of Shandong Province for L.P.X and Shandong Science Fund for Excellent Young Scholars (ZR2022YQ66), Academic Promotion Programme of Shandong First Medical University (No. 2019LJ003).

Availability of data and materials

The collected and analyzed datasets during this study are included in this manuscript.

Ethics approval and consent to participate

There are no any animal experiments and related animal ethical issues involved in this research article.

Consent for publication

All authors agree with the submission and publication of this paper.

Competing interests

The authors declare no competing interests.

References

1. Saftig P, Klumperman J. Lysosome biogenesis and lysosomal membrane proteins: trafficking meets function. Nat Rev Mol Cell Biol. 2009;10(9):623-635.
2. Banushi B, Joseph SR, Lum B, Lee JJ, Simpson F. Endocytosis in cancer and cancer therapy. Nat Rev Cancer. 2023;23(7):450-473.
3. Debnath J, Gammoh N, Ryan KM. Autophagy and autophagy-related pathways in cancer. Nat Rev Mol Cell Biol. 2023;24(8):560-575.
4. Watson J, Ferguson HR, Brady RM, Ferguson J, Fullwood P, Mo H, Bexley KH, Knight D, Howell G, Schwartz JM, et al. Spatially resolved phosphoproteomics reveals fibroblast growth factor receptor recycling-driven regulation of autophagy and survival. Nat Commun. 2022;13(1):6589.
5. Kirkegaard T, Jäättelä M. Lysosomal involvement in cell death and cancer. Biochim Biophys Acta. 2009;1793(4):746-754.
6. Jeswani G, Paul SD, Jha AK. Advances in the Delivery of Cancer Therapeutics: A Comprehensive Review. Curr Drug Deliv. 2018;15(1):21-36.
7. Vasan N, Baselga J, Hyman DM. A view on drug resistance in cancer. Nature. 2019;575(7782):299-309.
8. Hou DY, Wang MD, Zhang NY, Xu S, Wang ZJ, Hu XJ, Lv GT, Wang JQ, Lv MY, Yi L, et al. A Lysosome-Targeting Self-Condensation Prodrug-Nanoplatform System for Addressing Drug Resistance of Cancer. Nano Lett. 2022;22(10):3983-3992.
9. Hussein NA, Malla S, Pasternak MA, Terrero D, Brown NG, Ashby CR, Jr., Assaraf YG, Chen ZS, Tiwari AK. The role of endolysosomal trafficking in anticancer drug resistance. Drug Resist Updat. 2021;57:100769.
10. Stefan SM, Jansson PJ, Kalinowski DS, Anjum R, Dharmasivam M, Richardson DR. The growing evidence for targeting P-glycoprotein in lysosomes to overcome resistance. Future Med Chem. 2020;12(6):473-477.
11. de Klerk DJ, Honeywell RJ, Jansen G, Peters GJ. Transporter and Lysosomal Mediated (Multi)drug Resistance to Tyrosine Kinase Inhibitors and Potential Strategies to Overcome Resistance. Cancers (Basel). 2018;10(12):503.

12. Hraběta J, Belhajová M, Šubrtová H, Merlos Rodrigo MA, Heger Z, Eckschlager T. Drug Sequestration in Lysosomes as One of the Mechanisms of Chemoresistance of Cancer Cells and the Possibilities of Its Inhibition. Int J Mol Sci. 2020;21(12):4392.
13. Wang J, Hu L, Zhang H, Fang Y, Wang T, Wang H. Intracellular Condensates of Oligopeptide for Targeting Lysosome and Addressing Multiple Drug Resistance of Cancer. Adv Mater. 2022;34(1):e2104704.
14. Sun Z, Liu Q, Wang X, Wu J, Hu X, Liu M, Zhang X, Wei Y, Liu Z, Liu H, et al. Bioorthogonal catalytic nanozyme-mediated lysosomal membrane leakage for targeted drug delivery. Theranostics. 2022;12(3):1132-1147.
15. Ruzickova E, Skoupa N, Dolezel P, Smith DA, Mlejnek P. The Lysosomal Sequestration of Tyrosine Kinase Inhibitors and Drug Resistance. Biomolecules. 2019;9(11):675.
16. Sun Y, Sha Y, Cui G, Meng F, Zhong Z. Lysosomal-mediated drug release and activation for cancer therapy and immunotherapy. Adv Drug Deliv Rev. 2023;192:114624.
17. Pisa R, Kapoor TM. Chemical strategies to overcome resistance against targeted anticancer therapeutics. Nat Chem Biol. 2020;16(8):817-825.
18. Luo Y, Han Y, Hu X, Yin M, Wu C, Li Q, Chen N, Zhao Y. Live-cell imaging of octaarginine-modified polymer dots via single particle tracking. Cell Prolif. 2019;52(2):e12556.
19. Fu L, Zhang Y, Farokhzad RA, Mendes BB, Conde J, Shi J. 'Passive' nanoparticles for organ-selective systemic delivery: design, mechanism and perspective. Chem Soc Rev. 2023;52(21):7579-7601.
20. Madak JT, Cuthbertson CR, Miyata Y, Tamura S, Petrunak EM, Stuckey JA, Han Y, He M, Sun D, Showalter HD, Neamati N. Design, Synthesis, and Biological Evaluation of 4-Quinoline Carboxylic Acids as Inhibitors of Dihydroorotate Dehydrogenase. J Med Chem. 2018;61(12):5162-5186.
21. Chen Y, Yang T, Chen S, Qi S, Zhang Z, Xu Y. Silver nanoparticles regulate autophagy through lysosome injury and cell hypoxia in prostate cancer cells. Journal of Biochemical and Molecular Toxicology. 2020;34(5):e22474.
22. Chen Q, Shao X, Hao M, Fang H, Guan R, Tian Z, Li M, Wang C, Ji L, Chao H, et al. Quantitative analysis of interactive behavior of mitochondria and lysosomes using structured illumination microscopy. Biomaterials. 2020;250:120059.
23. Kirkegaard T, Roth AG, Petersen NH, Mahalka AK, Olsen OD, Moilanen I, Zylicz A, Knudsen J, Sandhoff K, Arenz C, et al. Hsp70 stabilizes lysosomes and reverts Niemann-Pick disease-associated lysosomal pathology. Nature. 2010;463(7280):549-553.
24. Borkowska M, Siek M, Kolygina DV, Sobolev YI, Lach S, Kumar S, Cho YK, Kandere-Grzybowska K, Grzybowski BA. Targeted crystallization of mixed-charge nanoparticles in lysosomes induces selective death of cancer cells. Nat Nanotechnol. 2020;15(4):331-341.
25. Wang Y, Wang YF, Li X, Wang Y, Huang Q, Ma X, Liang XJ. Nanoparticle-Driven Controllable Mitochondrial Regulation through Lysosome-Mitochondria Interactome. ACS Nano. 2022;16(8):12553-12568.

26. Barral DC, Staiano L, Guimas Almeida C, Cutler DF, Eden ER, Futter CE, Galione A, Marques ARA, Medina DL, Napolitano G, et al. Current methods to analyze lysosome morphology, positioning, motility and function. Traffic. 2022;23(5):238-269.
27. Fetterman JL, Holbrook M, Flint N, Feng B, Bretón-Romero R, Linder EA, Berk BD, Duess MA, Farb MG, Gokce N, et al. Restoration of autophagy in endothelial cells from patients with diabetes mellitus improves nitric oxide signaling. Atherosclerosis. 2016;247:207-217.
28. Yang MC, Shi XZ, Yang HT, Sun JJ, Xu L, Wang XW, Zhao XF, Wang JX. Scavenger Receptor C Mediates Phagocytosis of White Spot Syndrome Virus and Restricts Virus Proliferation in Shrimp. PLoS Pathog. 2016;12(12):e1006127.
29. Cao R, Li Y, Hu X, Qiu Y, Li S, Xie Y, Xu C, Lu C, Chen G, Yang J. Glycyrrhizic acid improves tacrolimus-induced renal injury by regulating autophagy. FASEB J. 2023;37(2):e22749.
30. Mohiuddin SG, Ghosh S, Kavousi P, Orman MA. Proton Motive Force Inhibitors Are Detrimental to Methicillin-Resistant Staphylococcus aureus Strains. Microbiol Spectr. 2022;10(4):e0202422.
31. Wang Y, Wang W, Xu L, Zhou X, Shokrollahi E, Felczak K, van der Laan LJ, Pankiewicz KW, Sprengers D, Raat NJ, et al. Cross Talk between Nucleotide Synthesis Pathways with Cellular Immunity in Constraining Hepatitis E Virus Replication. Antimicrob Agents Chemother. 2016;60(5):2834-2848.
32. Mao C, Liu X, Zhang Y, Lei G, Yan Y, Lee H, Koppula P, Wu S, Zhuang L, Fang B, et al. DHODH-mediated ferroptosis defence is a targetable vulnerability in cancer. Nature. 2021;593(7860):586-590.
33. Huang ZH, Qiao J, Feng YY, Qiu MT, Cheng T, Wang J, Zheng CF, Lv ZQ, Wang CH. Reticulocalbin-1 knockdown increases the sensitivity of cells to Adriamycin in nasopharyngeal carcinoma and promotes endoplasmic reticulum stress-induced cell apoptosis. Cell Cycle. 2020;19(13):1576-1589.
34. Sun Q, Xu W, Ji S, Qin Y, Liu W, Hu Q, Zhang Z, Liu M, Yu X, Xu X. Role of hepatocyte nuclear factor 4 alpha in cell proliferation and gemcitabine resistance in pancreatic adenocarcinoma. Cancer Cell Int. 2019;19:49.

Figures

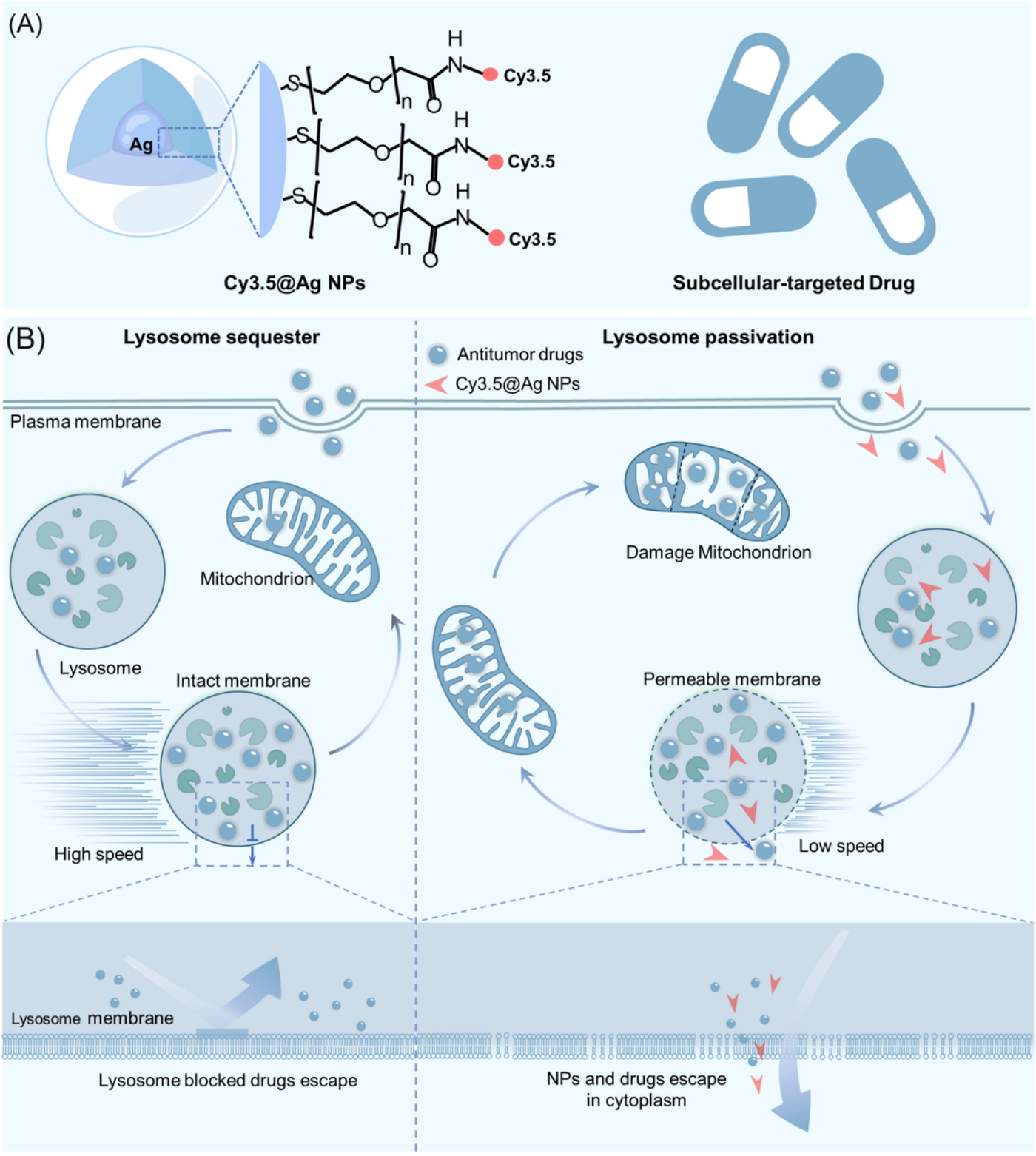

Figure 1

Schematic diagram of the structure and function of Cy3.5@Ag NPs for enhancing subcellular-targeted drug therapy. (A) Schematic illustration of the compositions of a Cy3.5@Ag NP. (B) Schematic illustration of drugs uptake by lysosomes and nanoparticles promoting drug release from lysosomes.

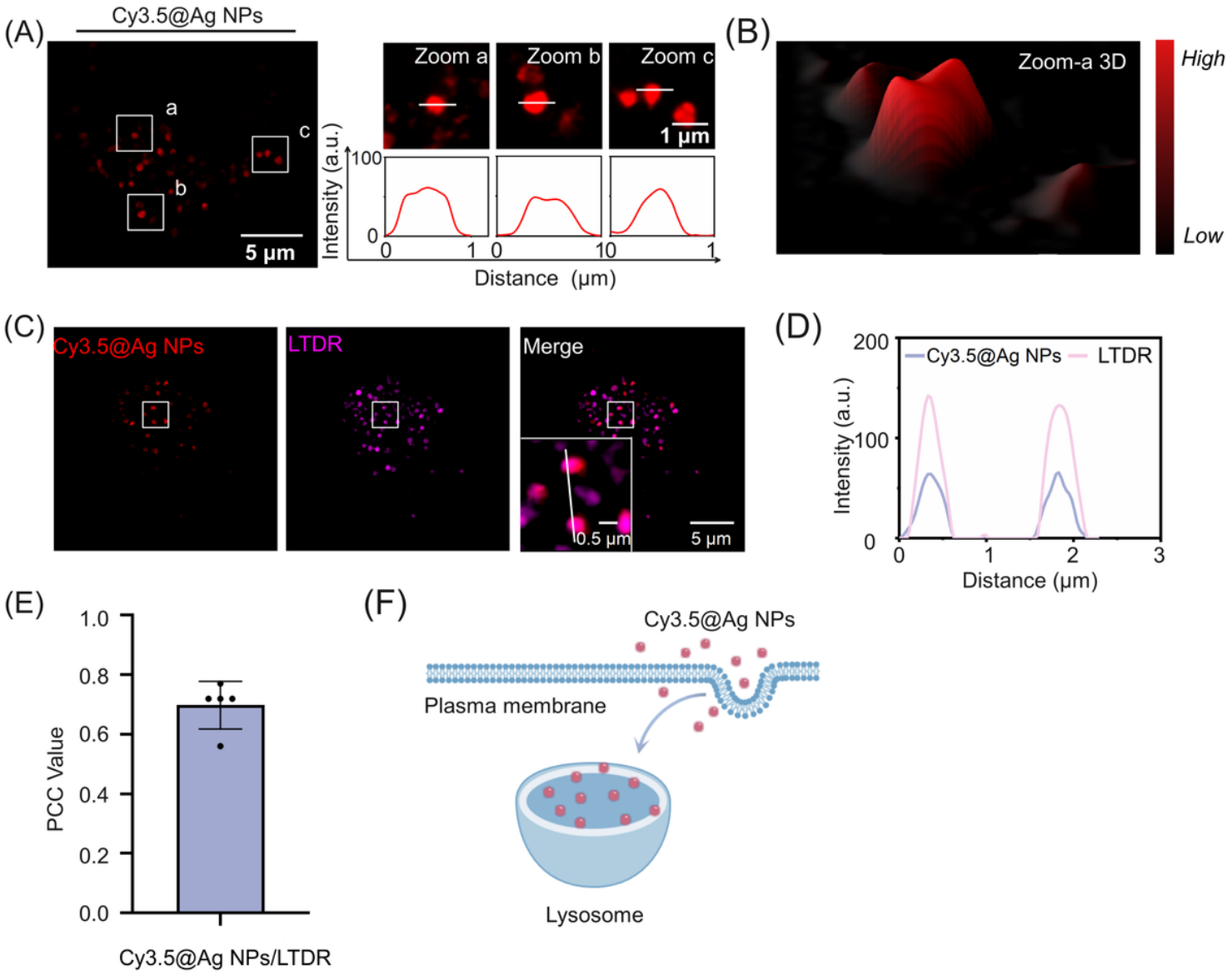

Figure 2

Localization of Cy3.5@Ag NPs in lysosomes. (A) Super-resolution images of HeLa cells incubated with **Cy3.5@Ag NPs** (0.5 μg/mL) for 1 h. Zoom-in images of regions of interest are presented in white rectangles. Plots show the fluorescence intensity of **Cy3.5@Ag NPs** in white line from zoom image. (B) 3D-fluorescence intensity image of figure zoom-a. (C) Fluorescence images of mitochondria in HeLa cells incubated with **Cy3.5@Ag NPs** (0.5 μg/mL) for 1 h and Lyso-Tracker Deep Red (LTDR, 100nM) for 30 min. (D) The fluorescence intensity of **Cy3.5@Ag NPs** and LTDR in white line from figure C. (E) PCC values of $LTDR^{640\text{-}690}/NPs^{488\text{-}590}$. (F) Schematic representation of lysosomes in living cells stained by **Cy3.5@Ag NPs**.

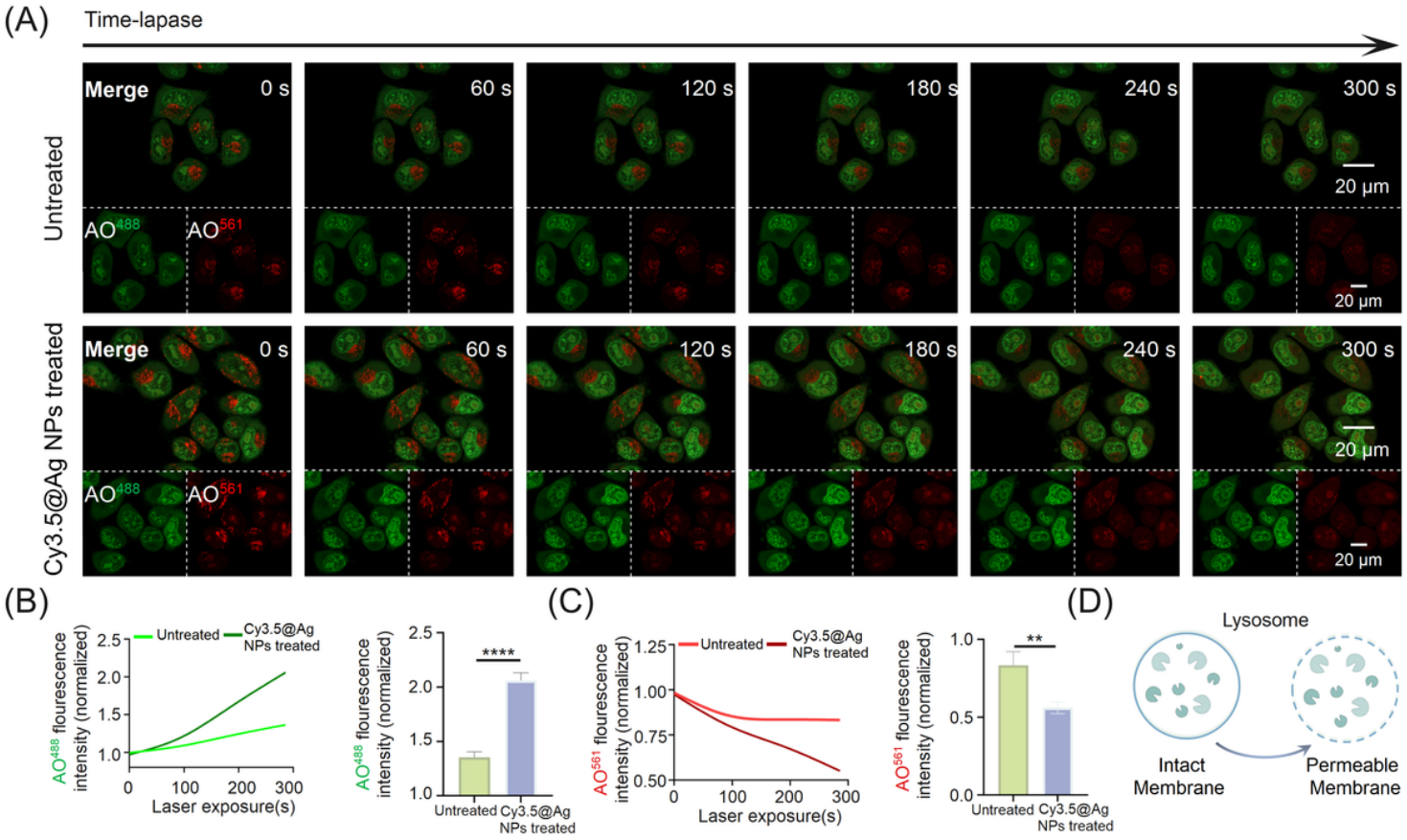

Figure 3

Cy3.5@Ag NPs induced lysosomal membrane permeabilization**. (**A) Time-dependent fluorescent images of acridine orange (AO, 2.0 μg/mL) by continuous exposure to blue laser light in HeLa cells with or without **Cy3.5@Ag NPs** (0.5 μg/mL) treatment. (B) Plots show AO leakage into the cytoplasm quantified as a rise in green fluorescence and as a decrease in red fluorescence. Data are presented as mean values. (C) The plots show the degree of change in AO fluorescence at the terminal moment from figure B. Data are presented as mean ± SEM. $P < 0.05$ is considered significant (**$P < 0.01$, ****$P < 0.0001$). (D) Schematic representation of lysosomal membrane permeabilization (LMP).

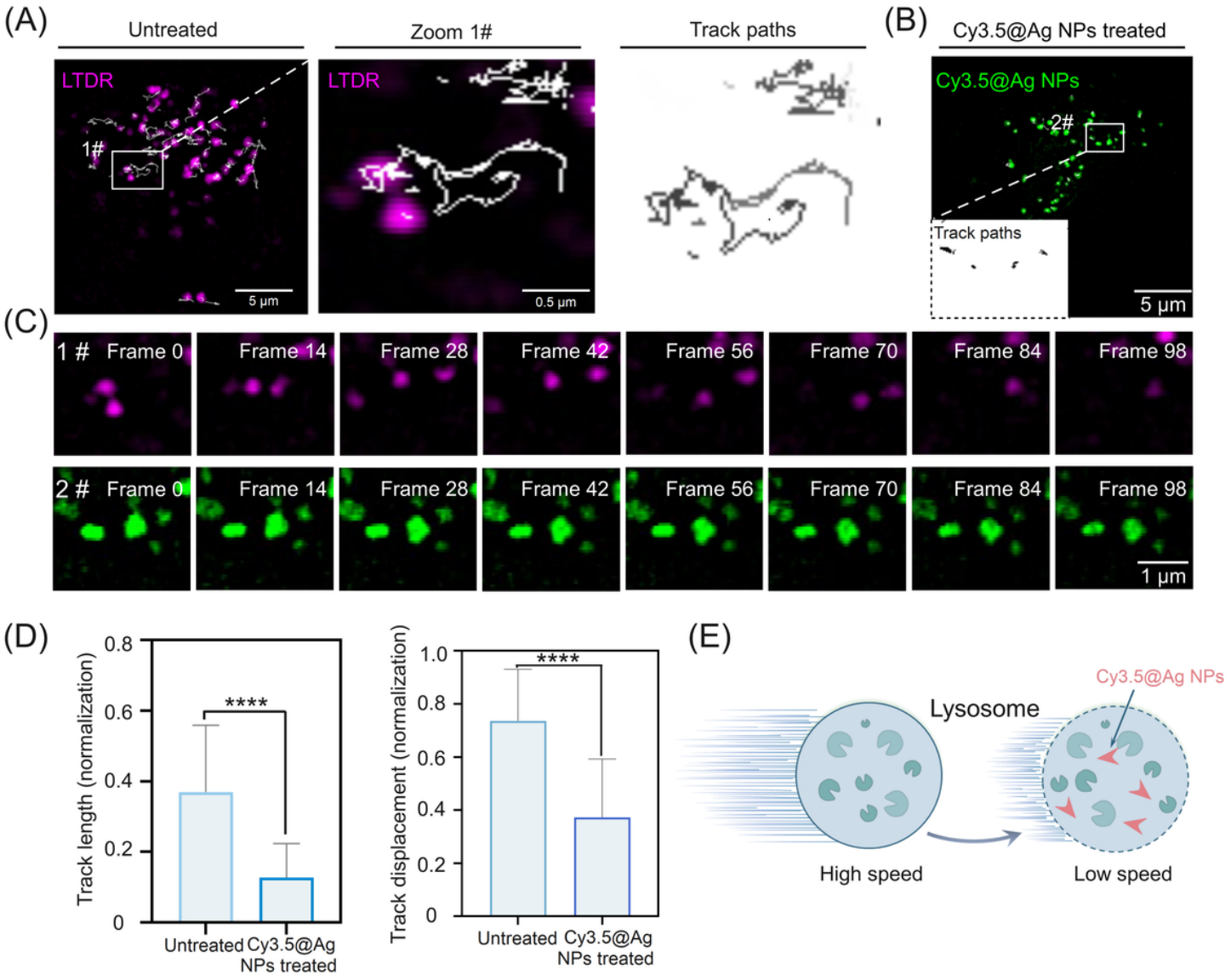

Figure 4

Cy3.5@Ag NPs induced lysosomal passivation. (A,B) Trajectories of lysosomal movements (shown in white) are superimposed over merged SIM snapshots from movies of lysosomes (LTDR, 100 nM, magenta, figure A) and **Cy3.5@Ag NPs** (0.5 μg/mL, green, figure B) in HeLa cells. (C) Time-dependent fluorescent images of LTDR-labeled lysosomes and **Cy3.5@Ag** NPs-labeled lysosomes in white rectangles from figure A and B. (D) Quantification of length and distance travel for multiple lysosomal trajectories. Data are presented as mean ± SEM. $P < 0.05$ is considered significant (n=55 random trajectories from 3 cells for every group. ****$P < 0.0001$, n.s. for no significant difference). (E) Schematic representation of lysosomal passivation.

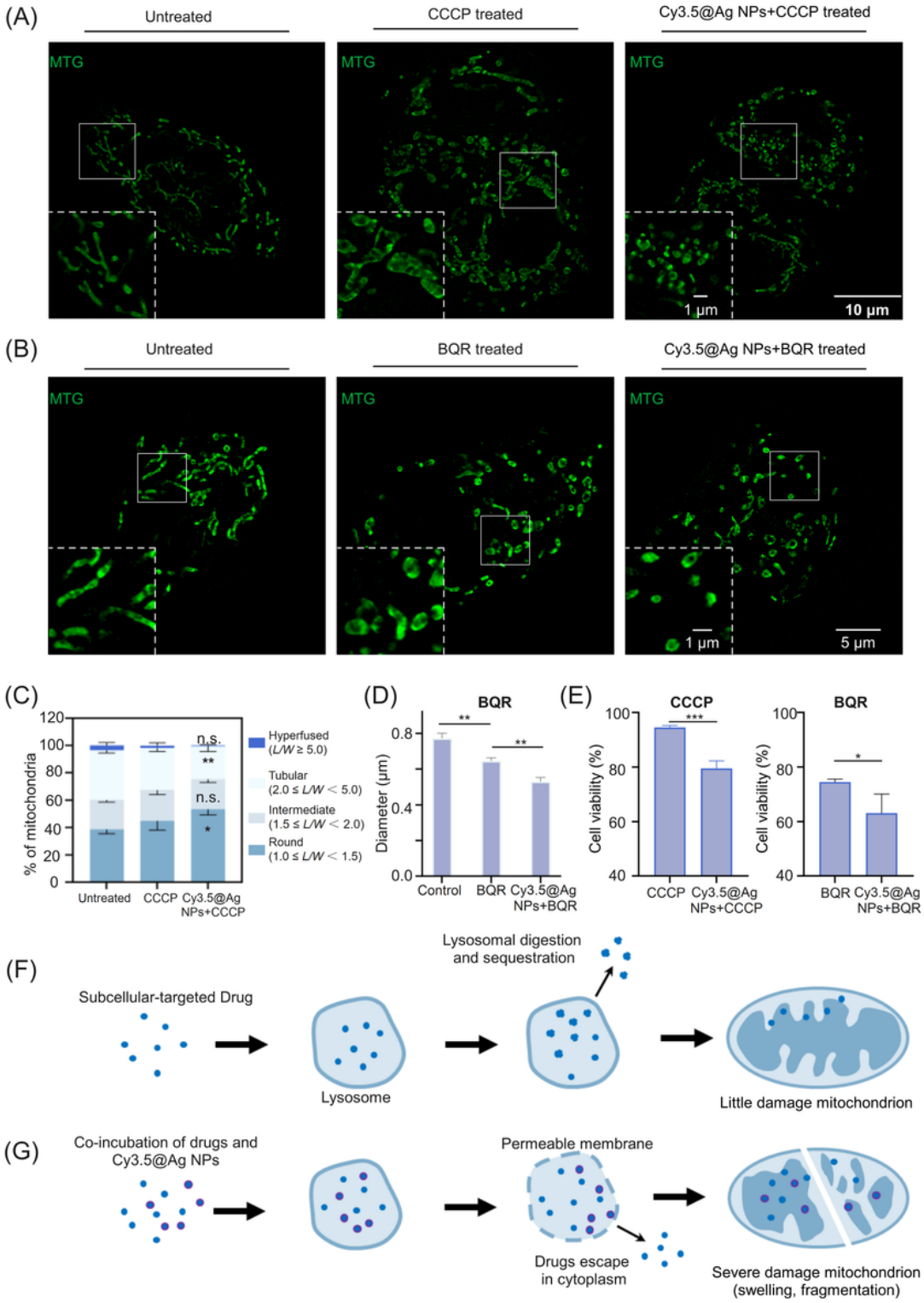

Figure 5

Cy3.5@Ag NPs enhances the mitochondria-targeted drugs for damaging mitochondrial morphology.(A) SIM imaging of HeLa cells co-stained by **Cy3.5@Ag NPs (**0.5 μg/mL**)** and MTG (100 nM) with or without CCCP (5 μM) treatment. White rectangles indicate Zoom-in image of region of interests. (B) SIM imaging of HeLa cells co-stained by **Cy3.5@Ag NPs** (0.5 μg/mL) and MTG (100 nM) with or without BQR (40 μM) treatment. White rectangles indicate Zoom-in image of region of interests. (C) Quantitative analysis of

mitochondrial morphology. Data as shown as mean ± SEM (n = 4 cells), $P < 0.05$ is considered significant (*$P < 0.05$, **$P < 0.01$, n.s. for no significant difference compared with CCCP treatment). (D) Mitochondrial morphology analysis of HeLa cells treated with BQR or **Cy3.5@Ag NPs**. Statistical analysis of mitochondrial particle size is shown in the plot. Data are presented as mean ± SEM, P < 0.05 is considered significant (**P< 0.01). (E) Cytotoxicity assay of the effect of CCCP and BQR on HeLa cells with or without **Cy3.5@Ag NPs**treatment. Data are presented as mean ± SEM. $P < 0.05$ is considered significant (*P < 0.05, ***P< 0.001). (F) Schematic representation of drugs which lack lysosomal escape capability. (G) Schematic representation of drugs co-incubation with **Cy3.5@Ag NPs**.

Supplementary Files

This is a list of supplementary files associated with this preprint. Click to download.

- wangxueqiansi.docx